Acta Polytechnica **64**(2):68–76, 2024
https://doi.org/10.14311/AP.2024.64.0068

Published by the Czech Technical University in Prague

P-LDPC CODED IMAGE TRANSMISSION WITH OFDM OVER UNDERWATER ACOUSTIC CHANNEL

Aymen M. Al-Kadhimi[a,*], Ammar E. Abdelkareem[b], Charalampos C. Tsimenidis[c]

[a] *Al-Nahrain University, College of Information Engineering, Department of Information and Communications Engineering, Al Jadriah, 10070 Baghdad, Iraq*

[b] *Al-Nahrain University, College of Information Engineering, Department of Computer Networks Engineering, Al Jadriah, 10070 Baghdad, Iraq*

[c] *Nottingham Trent University, School of Science and Technology, Department of Engineering, 50 Shakespeare Street, NG1 4FQ Nottingham, The United Kingdom*

[*] corresponding author: aymen.mohammed@nahrainuniv.edu.iq

Abstract. Underwater environment is still an attractive area to explore and exploit by human beings. However, underwater characteristics limit communications due to harsh channel conditions, and efficient channel codes are essential to deploy. This study presents an underwater system based on protograph low-density parity check (P-LDPC) codes and orthogonal frequency division multiplexing (OFDM) for image transmission. The system proves a successful reconstruction of P-LDPC coded images with different levels of comparison. The performance of the proposed system is evaluated using nine objective measures such as bit error rate (BER) and peak signal to noise ratio (PSNR). Firstly, the proposed system performance is evaluated with different block lengths of P-LDPC code. Then, the implemented system shows a coding gain of approximately 1.75 dB for applying P-LDPC when compared to polar with cyclic redundancy check at 0.0001 BER. Additionally, image subjective assessment is obtained to demonstrate how the P-LDPC outweighs polar and turbo product codes in terms of estimated image quality. Lastly, further investigation is performed to study the effect of varying fast Fourier transform (FFT) size and cyclic prefix (CP) length on image reserved quality. The results show that the received image is better reconstructed for larger FFT sizes since that produce longer CP and symbol duration, and that in turn helps the system to combat the multipath fading introduced by the underwater channel.

Keywords: Channel coding, P-LDPC, OFDM, underwater, polar code, bit error rate.

1. Introduction

The water covers the majority of our planet and has more to discover. That environment has attracted the researchers to explore underwater events using modern communications technologies. Autonomous underwater vehicles (AUVs), smart sensors, developed underwater communication technologies and routing protocols are all playing crucial roles in enabling humans to benefit from monitoring the quality of water and submarine creatures, exploring resources (e.g., oil and food) or even preparing for disasters [1].

Although the underwater environment offers advantages to humans, it also poses challenges for the development of reliable data transmission. Firstly, water tends to dampen electromagnetic signals which limits the transmission ranges due to signal attenuation. Thus, the acoustic signals are mostly devoted in underwater communication due to its longer transmission ranges [1]. Secondly, severe complicated propagation paths can be created with higher delays due to signals scattering/reflections which is known as multipath effect. This challenge can be mitigated by implementing the orthogonal frequency division multiplexing (OFDM) scheme which assists in eliminating multipath fading introduced by the channel. Thirdly, underwater node's movement caused by underwater currents regularly has negative impacts such as Doppler shifts in the received data which requires signal processing approach to compensate recovery [2]. Furthermore, the chaotic node mobility leads to instability in coverage [3] since the movement emerges holes in coverage and changes in topology and may even cause risks of collisions, therefore, node coordination/controlling algorithms can be deployed [4]. In consequence of those challenges, the quality of data transmission is affected in terms of reduced data rate to cope with complication in underwater channels and frequent increased data packet loss. Adopting coding schemes that focus on error correction to mitigate the channel's severe conditions is apparently essential for data integration enhancement in such environment.

In literature, the existing channel coding schemes for underwater acoustic communications (UAC) are apparently limited [5]. In [6], the Reem Solomon codes and convolutional codes were examined in the UAC environment. The authors developed robust

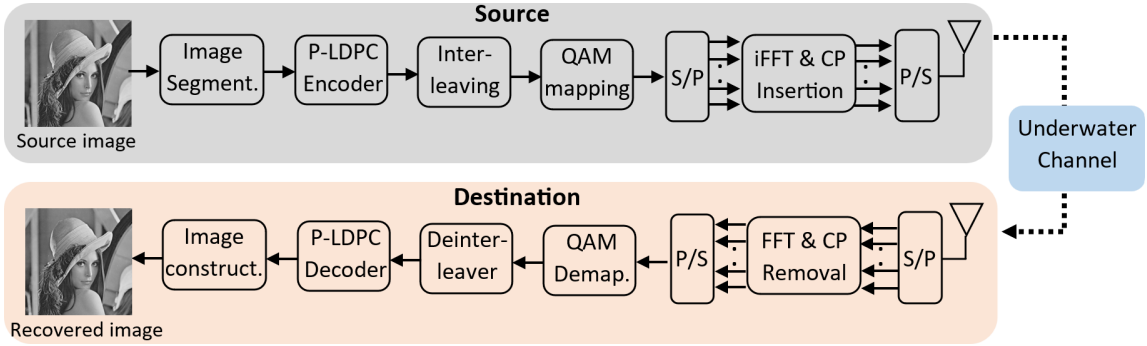

FIGURE 1. System design schematic.

acoustic channel that reliably permits transmitting text, images and low-bit-rate speech with the aid of an equalizer designed to mitigate channel impacts. In [7], space-time coding schemes were applied jointly with multipleinput-multiple-output (MIMO) systems for providing higher UAC transmission rate. In this study, trellis and layered codes were developed with an adaptive equalizer at receiver. The authors performed practical experiments on a real channel in the Pacific Ocean to prove a 48 kb/s of data rate can ben reliably transmitted in a 23 kHz bandwidth and over a 2 km range. In [8], LDPC codes for non-binary sources were investigated for underwater multicarrier communications. In [9], OFDM transmission was developed with adaptive-based modulation and coding systems. The results showed via real-time sea experiments that the transmission rate was maximized at a given designated power. In [10], P-LDPC codes were designed particularly for UAC channels. The simulation tests proved that the developed code was outperforming the MacKay's LDPC (3,6) codes by 0.5 dB coding gain at 0.00001 BER. Moreover, the study in [11] analyzed the transmission over UAC channels using extrinsic information transfer (EXIT). The finite-length EXIT, rather than traditional infinite-length EXIT, was developed for P-LDPC codes with 0.5 rate to show its outperformance compared with the (3,6) regular LDPC codes. The authors in [12] proposed a coding scheme in which source and channel coding is realized jointly to be applied for UAC using a deep learning approach. The authors proved via conducting simulations that their proposed deep learning approach can offer higher data rates than traditional mechanism in which the modulation with the source and channel coding are performed separately. Most recently, the paper [5] proposed a P-LDPC code designed for UAC in a differential chaotic bit-interleaved coded modulation (DC-BICM) system. The results showed that the proposed system compared with its counterparts can achieve 0.48 dB channel coding gain for P-LDPC with up to 69.5 % reduced number of iterations in average. In [13], the authors applied a protograph based spatially coupled LDPC (SC-LDPC) to evaluate its performance over UAC. The results showed that for the same latency constraints, SC-LDPC could achieve 1 dB gain compared with LDPC at 0.001 BER for data transmission over a shallow water channel with 10 kHz bandwidth.

On the other hand, several studies have considered the underwater image improvement. In [14], a summarization of underwater image quality enhancement methods was presented in two approaches: image formation model IFM-based and IFM-free. Particularly, for the latter category, the methods of enhancement primarily rely on redistributing image pixels to improve the contrast and coloring. IFM-free image improving techniques may involve pixel value manipulation into two aspects: spatial or transform domains. For the spatial approach, several studies have been proposed in this regard to deal with single-color [15] or multi-color [16]. For the transformed domain, the studies [17, 18] have suggested methods of improvements for single underwater images using wavelet transform. This technique allows for the coefficients of red-green-blue (RGB) components to be approximated and processed for image intensity adjustment and then image local contrast enhancement.

To the extent of our knowledge, the LDPC based on 5G-NR protograph construction for image transmission over underwater channels has not been investigated in literature yet. Consequently, this study aims to fill the aforementioned research gap by building an OFDM based underwater communication system with adopting a capacity-approaching P-LDPC error control coding scheme to safeguard image transmission over this harsh environment. The rest of the study is structured as follows. Section 2 presents the proposed communication system design. Section 3 shows the P-LDPC code structure and decoding algorithm. The simulation results and discussion are outlined in Section 4. Finally, the conclusion is drawn in Section 5.

2. System design

This paper proposes the system design as depicted in Figure 1. For the test standard images, many sets have been used in literature. In this study, the Lena gray image with 256 by 256 pixels is chosen as a standard test image being transmitted from the source to destination over an underwater channel.

Parameter	Value
Channel bandwidth	8 kHz
Max. delay spread	3.5 ms
Number of subcarriers	128
Symbol duration	16 ms
Spacing of subcarriers	62.5 Hz
Cyclic prefix duration	4 ms
Overall OFDM symbol duration	20 ms

Table 1. OFDM parameters.

Firstly, at the source (or transmitter), the source text image is segmented into smaller packets (or blocks) for post-processing. Then, the segmented data is attached with redundant control bits for channel coding using a P-LDPC code to combat the channel distortion. The encoded data are then permuted via an interleaver for the purpose of spreading out possible consecutive burst errors, and that contributes to enhancing the system performance. Afterwards, the symbols $x = [x(0), x(1), \cdots, x(M-1)]^T$ of length M are parallelised such that $x(i)$ represents the i-th symbol selected from a quadrature amplitude modulation (QAM) mapping. The OFDM stage comes next by performing inverse fast Fourier transform (iFFT) along with pilot pins and a cyclic prefix (CP) insertion so that inter-symbol interference (ISI) is eliminated at the destination. It is crucial for the CP length to be longer than the maximum channel delay. Therefore, the data symbols with N-length CP extension become as:

$$x_{\text{CP}} = [\underbrace{x(M-N+1), \ldots, x(M-1)}_{\text{CP}} \underbrace{x(0), x(1), \ldots, x(M-1)}_{x}]^T, \tag{1}$$

which then passes through a parallel to serial conversion (P/S) to be sequentially sent over an underwater channel.

In multipath channels, the transfer function of the channel is given as:

$$H(f) = \sum_p H_p(f) e^{-j2\pi f \tau_p}, \tag{2}$$

where at p$^{\text{th}}$ path ($p = 0, 1, 2, \ldots$)

$H_p(f)$ is the transfer function,

τ_p is the delay of propagation.

The channel impulse response can be written as:

$$h(t) = \sum_p h_p(t - \tau_p). \tag{3}$$

In this paper, the underwater acoustic channel is considered with the parameters listed in Table 1. The adopted channel is a baseband complex channel with 8 kHz bandwidth and 3.5 ms maximum delay spread.

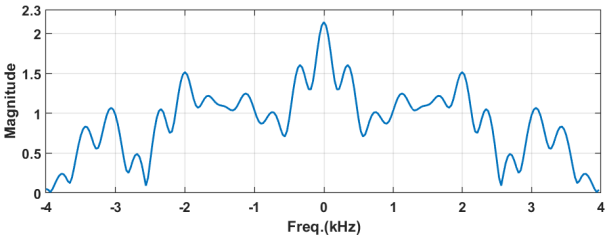

Figure 2. Underwater channel frequency response.

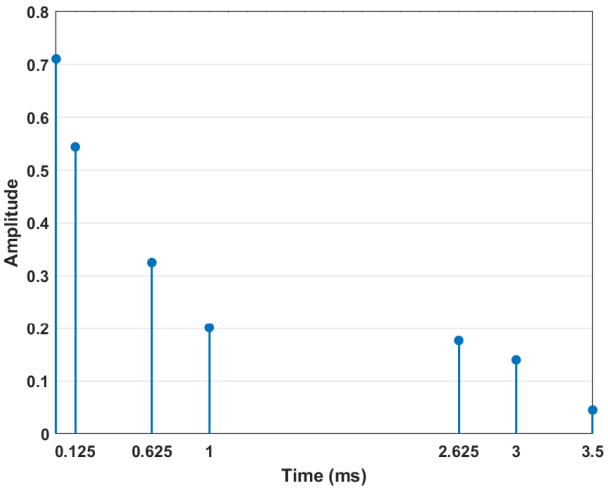

Figure 3. Underwater channel impulse response.

The underwater channel frequency response is shown in Figure 2. Moreover, the correspondence magnitude impulse response of the used underwater channel is depicted in Figure 3. That latter figure shows the multipath components with the associated delays and amplitudes. Equation (4) is used to calculate the root mean square (RMS) delay spread to be 0.64 ms:

$$\tau_{\text{rms}} = \sqrt{\frac{\sum_p ((t_p - t_a) - \tau_m)^2 a_p^2}{\sum_p a_p^2}}, \tag{4}$$

where

t_p is the arrival time of the p$^{\text{th}}$ path,

t_a is the arrival time of the first path,

a_p is the amplitude of the p$^{\text{th}}$ path,

τ_m is the average delay obtained as:

$$\tau_m = \frac{\sum_p (t_p - t_a) a_p^2}{\sum_p a_p^2}. \tag{5}$$

The OFDM setting is shown in Table 1. The FFT length is set to 128. That means the 8 kHz bandwidth channel is subdivided into 128 sub-channels with a spacing of 62.5 Hz with 16 ms symbol duration. Furthermore, the CP duration is selected to be 4 ms, which is longer than the maximum delay spread of the underwater channel. That results in each sub-channel experiencing flat-fading and helps to reconstruct the received data.

Subsequently, the data received from the k$^{\text{th}}$ sub-channel are formed as:

$$y[k] = H[k]x[k] + n[k], \tag{6}$$

where

$H[k]$ is the transfer function,

$x[k]$ is the transmitted data,

$n[k]$ is the additive noise each associated with k$^{\text{th}}$ sub-channel for $k = 0, 1, 2, \ldots, 128$.

Then, the received vectors are parallelised before passing through the FFT and CP removal operations. Preultimately, de-mapping, de-interleaving, and channel decoding are executed sequentially. Lastly, the data bits are reconstructed to produce back the estimated version of the 256×256 Lena image.

The performance objective measures used to evaluate the received data are mainly:

(1.) the bit error rate (BER) as the ratio of transmitted bits to the recovered bits,

(2.) the peak signal to noise ratio (PSNR) in dB, which is obtained as [19]:

$$\begin{aligned}&\text{PSNR}(M_t, M_r)\\ &= 10\log_{10}\left(mn\left(\frac{\max\left(M_t^2(i,j)\right)}{\sum_{i,j}\left[M_t(i,j) - M_r(i,j)\right]^2}\right)\right),\end{aligned} \tag{7}$$

where M_t and M_r are the $n \times m$ transmitted and received images, respectively. Furthermore, other measures are presented in the results and discussion section.

3. P-LDPC DESIGN

The channel coding scheme used in this paper is the LDPC code based on protograph construction that is defined by the 3rd generation partnership project (3GPP) in the fifth-generation new radio 5G-NR standard [20]. The construction of the LDPC H matrix is achieved by selecting one of two base graphs (BG) matrices (B_1 or B_2). The size of B_1 is 46×68 while B_2 is 42×52. The H matrix is created through the replacement of each element in B by a matrix with size $Z_c \times Z_c$, where Z_c is a lifting (or expansion) factor defined in the standard according to a set index. A detailed description of protograph construction and encoding phases is given with examples in [21].

For the decoding of P-LDPC used in this study, the offset min-sum MS (OMS) algorithm [22] is applied with a correction-factor (α) added directly to the log-likelihood ratio (LLR) outputs of the check nodes (CNs) as will be shown in the algorithm below. First, the codeword $C = \{c_1\ c_2\ \ldots\ c_I\}$ is categorised by a $J \times I$ parity-check matrix of an LDPC code. The symbol vector passes through the channel to produce r_i as an input to the P-LDPC decoder. Then, the soft-in-soft-output (SISO) iterative decoding is performed based on the LLRs exchanged between the variable nodes (VNs) and CNs, and that message passing mechanism is prompted by the decoding algorithm defined below. The set of VNs contributed in CN (cn_j) is established as $M(j) = \{i \mid h_{i,j} = 1\}$. Similarly, the set of CNs involved in VN (vn_i) is symbolised as $N(i)$. Furthermore, L_{ij} and L_{ji} are the two vectors representing the LLR information sent from the variable-node vn_i to the check-node cn_j or vice-versa from the check-node cn_j to the variable-node vn_i, respectively.

The OMS algorithm is described as:

Step 1 (Initialisation)

For k=0 and for each vn_i, $i \in [1, I]$:

$$L_{ij}^0 = r_i.$$

Step 2 (CN calculation)

Update cn_j, $j \in [1, J]$:

$$L_{ji,\text{MS}}^k = \left(\prod_{i' \in M(j)\setminus i} \text{sign}\left(L_{i'j}^{k-1}\right)\right) \cdot \min_{i' \in M(j)\setminus i}\left|L_{i'j}^{k-1}\right|,$$

$$L_{ji}^k = \max\left\{\left|L_{ji,\text{MS}}^k\right| - \alpha, 0\right\}.$$

Step 3 (VN calculation)

The k$^{\text{th}}$ output of vn_i, $i \in [1, I]$:

$$L_i^k = L_i^0 + \sum_{j \in N(i)} L_{ji}^k,$$

$$c_i^k = \left(1 - \text{sign}\left(L_i^k\right)\right)/2;\ X^k = C^k H^T,$$

if $X^k = 0$,

finalise decoding and assign the output $\widetilde{C} = C^k$.

Step 4

Update vn_i, $i \in [1, I]$:

$$L_{ij}^k = L_i^k - L_{ji}^k,\ j \in N(i),$$

increase k, then go to Step 2.

In terms of VNs and CNs update exchange, there are two scheduling mechanisms: flooding and layering. The latter mechanism is supported by the 5G-NR standard to provide a better performance with less complexity by requiring fewer iterations at the decoder to converge. That is because the layered decoders essentially group the H's rows into a certain number of bundles, each named a layer. For example, Equation (8) shows an H parity matrix whose rows are clustered to create two layers with C_1 & C_2 codes declared with H_1 & H_2 matrices, respectively. Its corresponding layered decoding is illustrated in Figure 4 where the LLRs denote variable-node updates [21]. The decoding mechanism is performed in a layered manner by initialising the decoder of C_1 with a channel LLR, then applying the LLR_{21} in the subsequent iterations. In a manner that is similar to the shown example, in this study, the base graph 2 (i.e., B_2) matrix is considered to have 42 layers/rows to guarantee layered processing of decoders in the 5G standard.

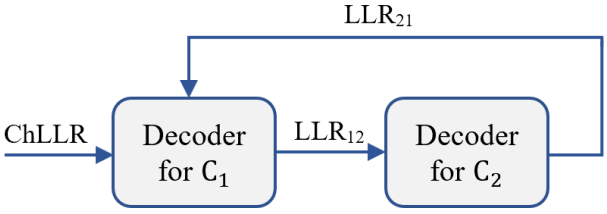

FIGURE 4. Example of layered decoding structure [21].

This layering mechanism allows for updated LLR messages on a layer to be used within the same iteration to perform new CN computations, rather than waiting for all column and row computations to produce newer messages [23]. Accordingly, the layered OMS decoding was implemented in this paper.

$$H = \begin{bmatrix} H_1 \\ H_2 \end{bmatrix} = \begin{bmatrix} 1 & 1 & 1 & 0 & 1 & 0 & 0 \\ 0 & 0 & 0 & 1 & 0 & 1 & 1 \\ 1 & 1 & 0 & 1 & 0 & 0 & 1 \\ 0 & 0 & 1 & 0 & 1 & 1 & 0 \end{bmatrix} \begin{matrix} \} \text{layer 1} \\ \\ \} \text{layer 2} \end{matrix} \quad (8)$$

4. RESULTS AND DISCUSSIONS

For the P-LDPC code, base graph 2, with different lifting (expansion) factor Z_c and layered OMS decoding were chosen for evaluation purposes. For a comparison with other coding schemes, polar coding [24] and block turbo codes [25] were implemented. For polar codes, the successive cancellation list (SCL) [26] decoding algorithm was realised with list sizes 4 and 8 along with the aid of an 11-bit cyclic redundancy check (CRC) [20] embedded within blocks of 1024 bits. For block turbo codes, a serial concatenation of extended Bose-Chaudhuri-Hocquenghem (BCH) code with extended Hamming code were selected to produce a 2-dimension turbo product code (2-D TPC) to offer 1056-bit block lengths. The block length values for polar and turbo codes were chosen for a fair comparison with 1.1k bit P-LDPC codes, and all schemes were implemented at 1/3 encoding rate. Additionally, the underwater nodes in this paper were considered as semi-static, and hence the mobility and Doppler effect are minimised.

Firstly, the performance of transmitting a P-LDPC coded image over an underwater channel for different block lengths are evaluated in terms of BER and PSNR as shown in Figure 5 and Figure 6, respectively. The block lengths were set as $n = 1.1$k, 2.3k, 4.6k and 9.2k bits, where k refers to a thousand, by doubling the Z_c from 36 to 72, 144, and 288, respectively. Figure 5 indicates that the designed system is performing well by estimating the received image with minimised errors for different block lengths with a higher signal to noise ratio (SNR). The system BER shows that although the behaviour of all four block lengths stays converged for lower SNRs, a divergence between them is explicitly shown in Figure 5 for the region above 2 dB. The longer the block

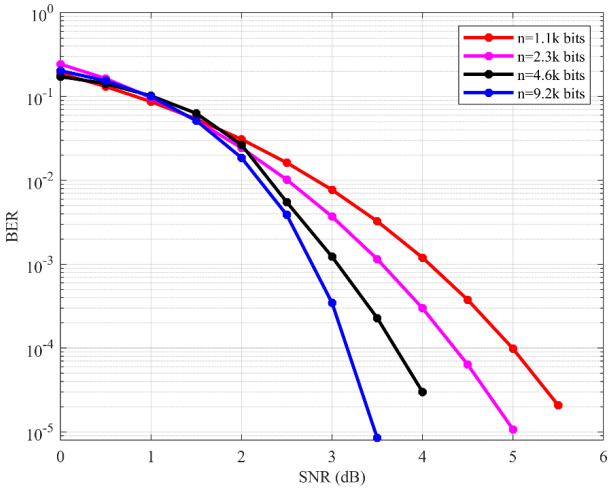

FIGURE 5. BER of P-LDPC coded image transferred over underwater channel with different block lengths.

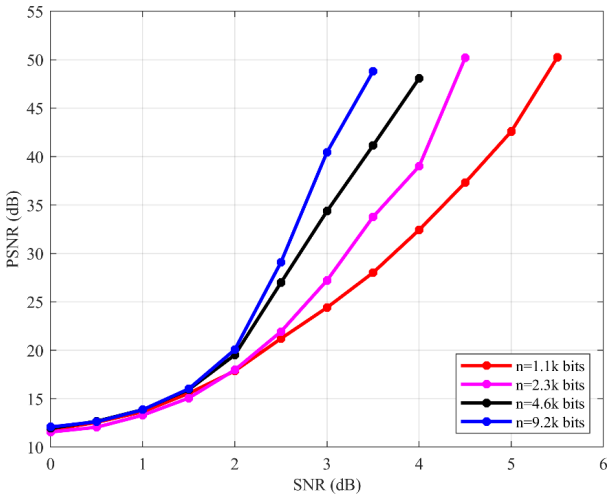

FIGURE 6. PSNR of P-LDPC coded image transferred over underwater channel with different block lengths.

length, the better the BER performance. For example, at SNR = 3.5 dB, the system performs the best at the block length $n = 9.2$k bits to offer less than 10^{-5} BER as compared to 0.002, 0.001 and 0.0002 at $n = 1.1$k, 2.3k and 4.6k bits, respectively. Similarly, Figure 6 shows the system performance with various block lengths but in terms of PSNR (in dB) rather than BER. Similar indication is revealed, the increase in block length results in an increase in PSNR between the transmitted and received images, which means a better system behaviour. For example, in order for the system to achieve a PSNR of approximately 50 dB, P-LDPC with $n = 1.1$k bit length requires 5.5 dB of SNR compared to almost 3.6 dB SNR required by the code with $n = 9.2$k bit length. However, the code with block length of $n = 1.1$k bits can still achieve acceptable levels of BER and PSNR for a system transmitting images over a harsh underwater channel. Furthermore, the tradeoff between the block length and code complexity is a crucial matter to consider in an underwater environment where the system design

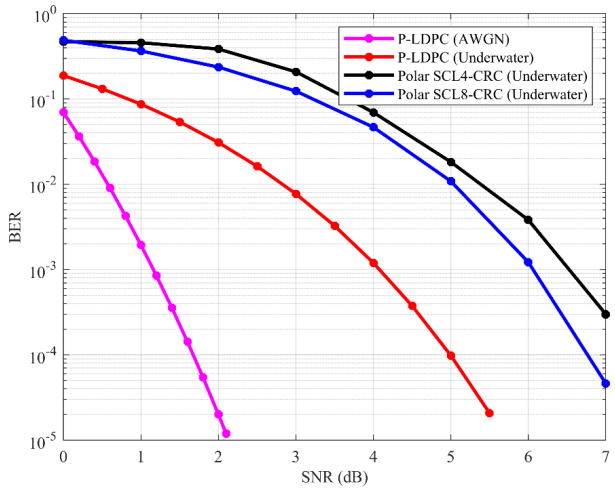

FIGURE 7. BER of coded image transferred over underwater channel with different coding schemes.

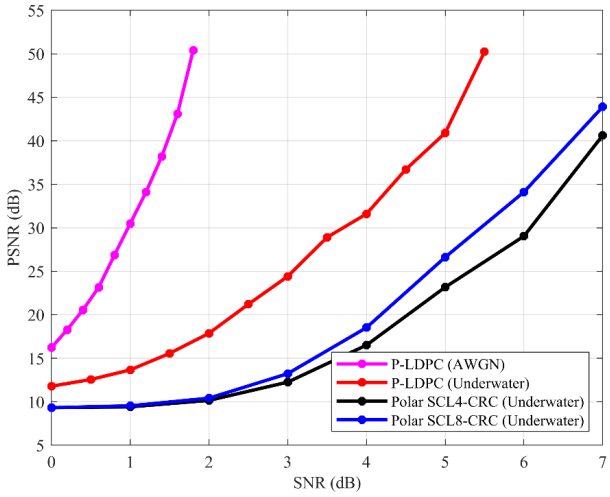

FIGURE 8. PSNR of coded image transferred over underwater channel with different coding schemes.

is highly constrained. In consequence, the shorter P-LDPC with $n = 1.1$k bits is further investigated for the rest of this section.

Secondly, the system behaviour is evaluated for images coded with P-LDPC and Polar SCL-CRC (list sizes 4 and 8) over an underwater channel. As the idea of list decoding of polar code is to make the SC decoders work as parallel groups, the list size of this technique plays a significant role in improving the code error correction capability. This principle is demonstrated in Figure 7 where the Polar SCL-CRC size 8 outperforms the size 4 in terms of BER at the same SNR. Moreover, Figure 7 shows that P-LDPC accomplishes better BER than Polar SCL8-CRC. For instance, there is a coding gain of approximately 1.75 dB for applying P-LDPC compared to Polar SCL8-CRC at 0.0001 BER. A similar comparison of these coding schemes but in terms of PSNR is demonstrated in Figure 8. The red curve represents the PSNR against SNR for P-LDPC code which can reach the peak at 50 dB PSNR at 5.5 dB SNR, which steadily outperforms Polar codes with both list sizes as depicted in Figure 8.

Thirdly, in addition to BER and PSNR, other performance measures are examined to further investigate image transmission over the underwater channel. Mean squared error (MSE), average difference (AD), structural content (SC), normalised cross-correlation (NK), maximum difference (MD), Laplacian MSE (LMSE), and normalised absolute error (NAE) are all calculated between the $n \times m$ transmitted image (M_t) and $n \times m$ received estimated image (M_r). As the performance of P-LDPC is more comparable to Polar SCL8-CRC, those other image measures are obtained in Table 2 for SNR values ranging from 0 dB to 5 dB. It is noticeable that the error-related measures (i.e. MSE, LMSE and NAE) are getting lower as the SNR values are increasing, and P-LDPC shows a faster decrease which indicates a better behaviour compared to Polar code. For AD and MD, the difference between the original and reconstructed images is minimal at higher SNR values, and again, P-LDPC has an advantage over Polar code. Lastly, for SC and NK measures, both are approaching 1 at higher SNR values, which reflects a higher similarity between the original image and the reconstructed estimated image.

Finally, after presenting various objective image measures, a subjective assessment is examined. This examination is done based on human observation to judge the estimated image quality as shown in Figure 9. The first comparison of the reconstructed images is performed for P-LDPC with different block lengths as shown in Figure 9a. The image quality is observed to be getting better as the block length is increasing for a fixed SNR value at 3 dB, with the difference being quite noticeable. Furthermore, Figure 9b shows the quality of the estimated P-LDPC coded image with different FFT sizes used in the OFDM system when performing iFFT and FFT at the transmitter and receiver, respectively. The FFT sizes are chosen to produce 64, 128, 256, and 512 subcarriers with CP lengths of one quarter of the symbol length for all sizes. The SNR value and block length are fixed at 4 dB and 1.1k bits, respectively, for a fair and recognisable comparison. Figure 9b demonstrates that the image quality is better for bigger FFT sizes as moving from 64-FFT to 128-FFT, 256-FFT, and 512-FFT will result in doubling the symbol durations from 8 ms to 16 ms, 32 ms and 64 ms, respectively. In consequence, the CP duration is increasing, which in turn helps the system to better combat the multipath fading introduced by the underwater channel. However, although the bigger FFT size results in a better performance, it adds more complexity as a trade-off. Lastly, Figure 9c compares the estimated image quality coded with P-LDPC, Polar, and 2-D TPC schemes. It is clear that the subjective judgement of the best quality is towards the P-LDPC when compared for 5 dB SNR and 1.1k bit block length.

SNR [dB]		0	1	2	3	4	5
MSE	P-LDPC	4307	2797	1061	235	45	5
	Polar-SCL8	7610	7234	5968	3096	962	165
AD	P-LDPC	−1.36	−0.241	−0.186	0.0314	−0.038	0.022
	Polar-SCL8	−4.08	−2.74	−2.09	0.919	0.549	0.0271
SC	P-LDPC	0.8946	0.9367	0.972	0.9953	0.9985	1.0002
	Polar-SCL8	0.81183	0.83135	0.8576	0.92556	0.9721	0.9955
NK	P-LDPC	0.9362	0.954	0.9841	0.9956	0.9994	0.9997
	Polar-SCL8	0.89918	0.89542	0.91307	0.95203	0.9869	0.9975
MD	P-LDPC	226	224	208	200	200	136
	Polar-SCL8	223	226	226	225	215	208
LMSE	P-LDPC	86.87	58.526	23.369	5.434	1.006	0.12
	Polar-SCL8	128.98	125.27	103.96	59.303	19.633	3.6931
NAE	P-LDPC	0.3291	0.2134	0.0819	0.0178	0.0031	0.0004
	Polar-SCL8	0.57933	0.55281	0.45435	0.2397	0.0744	0.0135

Table 2. Other objective image measures.

(a). P-LDPC coded at SNR = 3 dB and 128-FFT (for n = 1.1k, 2.3k, 4.6k, 9.2k from left to right).

(b). P-LDPC coded at SNR = 4 dB and n = 1.1k (for 64-FFT, 128-FFT, 256-FFT, 512-FFT from left to right).

(c). Various coding schemes at SNR = 5 dB and n = 1.1k (for 2-D TPC, Polar SCL-4, Polar SCL-8, P-LDPC from left to right).

Figure 9. Reconstructed image with various coding schemes over underwater.

5. Conclusion

This study presents an approach for transmitting images over an OFDM underwater channel based on P-LDPC coding schemes. The performance of the proposed system with P-LDPC is compared with other coding schemes and evaluated using both objective and subjective assessments of the quality of the reconstructed received image. The results show how implementing channel coding schemes can help combat transmission impairments caused by harsh underwater conditions. In addition, it is proved that the longer block lengths offer a better performance in terms of BER and PSNR. Furthermore, for a fixed SNR and block length, the size of FFT plays a crucial role in helping the system eliminate multipath fading introduced by the channel. Finally, the proposed system demonstrates its functionality for this type of harsh characteristic channels with reasonable levels of error rates and image quality at moderate SNRs.

For future work, some aspects can be more investigated. Fundamentally, real hardware implementation is lacking for further validation. Since the P-LDPC decoder performs iteratively, it is recommended to implement the proposed system using either the SHARC ADSP-21469 kit or the field programmable gate array (FPGA), which offers parallelism that suits the iterative coding nature. From the channel coding's side, the insertion of CRC bits to the P-LDPC is expected to further enhance its performance. Moreover, since the source coding is not one of the main points of focus in this paper, effective compressors are not realised. Consequently, implementing effective image compression schemes such as Better Portable Graphics (BPG) or Set Partitioning in Hierarchical Trees (SPIHT) will help minimising the size of the transmitted bits by removing image pixel redundancy. Accordingly, the system coding rate in general becomes increasable while maintaining the error correction performance. In other words, the rise in code rate enables the system to send more useful information bits, which in turn increases the system throughput and spectral efficiency that is essential in harsh underwater conditions. Finally, this study can be extended to the use of P-LDPC in the Internet of Underwater Things (IoUT) with dynamic network and higher node mobility. That will require to adopt adaptive compensation mechanisms against severe Doppler shift and self-interference cancellation systems with a novel pilot insertion technique [27].

References

[1] T. Qiu, Z. Zhao, T. Zhang, et al. Underwater internet of things in smart ocean: System architecture and open issues. *IEEE Transactions on Industrial Informatics* **16**(7):4297–4307, 2020. https://doi.org/10.1109/TII.2019.2946618

[2] A. Amar, G. Avrashi, M. Stojanovic. Low complexity residual Doppler shift estimation for underwater acoustic multicarrier communication. *IEEE Transactions on Signal Processing* **65**(8):2063–2076, 2017. https://doi.org/10.1109/TSP.2016.2630039

[3] W. Kim, H. W. Moon, Y. J. Yoon. Adaptive triangular deployment of underwater wireless acoustic sensor network considering the underwater environment. *Journal of Sensors* **2019**:6941907, 2019. https://doi.org/10.1155/2019/6941907

[4] W. Zhang, J. Wang, G. Han, et al. A cluster sleep-wake scheduling algorithm based on 3D topology control in underwater sensor networks. *Sensors* **19**(1):156, 2019. https://doi.org/10.3390/s19010156

[5] Z. Xu, Q. Chen, Y. Li, et al. Designing protograph LDPC codes for differential chaotic bit-interleaved coded modulation system for underwater acoustic communications. *Journal of Marine Science and Engineering* **11**(5):914, 2023. https://doi.org/10.3390/jmse11050914

[6] A. Goalic, J. Trubuil, N. Beuzelin. Channel coding for underwater acoustic communication system. In *OCEANS 2006*, pp. 1–4. 2006. https://doi.org/10.1109/OCEANS.2006.307093

[7] S. Roy, T. M. Duman, V. McDonald, J. G. Proakis. High-rate communication for underwater acoustic channels using multiple transmitters and space-time coding: Receiver structures and experimental results. *IEEE Journal of Oceanic Engineering* **32**(3):663–688, 2007. https://doi.org/10.1109/JOE.2007.899275

[8] J. Huang, S. Zhou, P. Willett. Nonbinary LDPC coding for multicarrier underwater acoustic communication. *IEEE Journal on Selected Areas in Communications* **26**(9):1684–1696, 2008. https://doi.org/10.1109/JSAC.2008.081208

[9] L. Wan, H. Zhou, X. Xu, et al. Adaptive modulation and coding for underwater acoustic OFDM. *IEEE Journal of Oceanic Engineering* **40**(2):327–336, 2015. https://doi.org/10.1109/JOE.2014.2323365

[10] Z. Chen, X. Xu, Y. Chen. Application of protograph-based LDPC codes in underwater acoustic channels. In *2014 IEEE International Conference on Signal Processing, Communications and Computing (ICSPCC)*, pp. 923–927. 2014. https://doi.org/10.1109/ICSPCC.2014.6986332

[11] Z. Chen, X. Xu, Y. Chen. Finite-length EXIT analyses for protograph LDPC codes over underwater acoustic channels. In *2017 IEEE International Conference on Signal Processing, Communications and Computing (ICSPCC)*, pp. 1–6. 2017. https://doi.org/10.1109/ICSPCC.2017.8242532

[12] Y. Inoue, D. Hisano, K. Maruta, et al. Deep joint source-channel coding and modulation for underwater acoustic communication. In *2021 IEEE Global Communications Conference (GLOBECOM)*, pp. 1–7. 2021. https://doi.org/10.1109/GLOBECOM46510.2021.9685931

[13] S. K. Padala, J. D'Souza. Performance of spatially coupled LDPC codes over underwater acoustic communication channel. In *2020 National Conference on Communications (NCC)*, pp. 1–5. 2020. https://doi.org/10.1109/NCC48643.2020.9056068

[14] Y. Wang, W. Song, G. Fortino, et al. An experimental-based review of image enhancement and image restoration methods for underwater imaging. *IEEE Access* **7**:140233–140251, 2019. https://doi.org/10.1109/ACCESS.2019.2932130

[15] C. O. Ancuti, C. Ancuti, C. De Vleeschouwer, P. Bekaert. Color balance and fusion for underwater image enhancement. *IEEE Transactions on Image Processing* **27**(1):379–393, 2018. https://doi.org/10.1109/TIP.2017.2759252

[16] A. S. Abdul Ghani, N. A. Mat Isa. Automatic system for improving underwater image contrast and color through recursive adaptive histogram modification. *Computers and Electronics in Agriculture* **141**:181–195, 2017. https://doi.org/10.1016/j.compag.2017.07.021

[17] A. Khan, S. S. A. Ali, A. S. Malik, et al. Underwater image enhancement by wavelet based fusion. In *2016 IEEE International Conference on Underwater System Technology: Theory and Applications (USYS)*, pp. 83–88. 2016. https://doi.org/10.1109/USYS.2016.7893927

[18] S. Vasamsetti, N. Mittal, B. C. Neelapu, H. K. Sardana. Wavelet based perspective on variational enhancement technique for underwater imagery. *Ocean Engineering* **141**:88–100, 2017. https://doi.org/10.1016/j.oceaneng.2017.06.012

[19] H. Kasban, M. A. M. M. K. El-Bendary. Performance improvement of digital image transmission over mobile WiMAX networks. *Wireless Personal Communications* **94**(3):1087–1103, 2017. https://doi.org/10.1007/s11277-016-3671-4

[20] ETSI 3rd Generation Partnership Project, Technical Specification Group Radio Access Network. 5G; NR; Multiplexing and channel coding (3GPP TS 38.212 version 17.1.0 release 17), 2022.

[21] A. M. Al-Kadhimi, A. E. Abdulkareem, C. C. Tsimenidis. Performance enhancement of LDPC codes based on protograph construction in 5G-NR standard. *Tikrit Journal of Engineering Sciences* **30**(4):1–10, 2023. https://doi.org/10.25130/tjes.30.4.1

[22] J. Chen, M. P. C. Fossorier. Near optimum universal belief propagation based decoding of low-density parity check codes. *IEEE Transactions on Communications* **50**(3):406–414, 2002. https://doi.org/10.1109/26.990903

[23] Z. Zhou, K. Peng, A. Krylov, et al. Enhanced adaptive normalized min-sum algorithm for layered scheduling of 5G-NR LDPC codes. In *2020 IEEE International Symposium on Broadband Multimedia Systems and Broadcasting (BMSB)*, pp. 1–5. 2020. https://doi.org/10.1109/BMSB49480.2020.9379739

[24] E. Arikan. Channel polarization: A method for constructing capacity-achieving codes for symmetric binary-input memoryless channels. *IEEE Transactions on Information Theory* **55**(7):3051–3073, 2009. https://doi.org/10.1109/TIT.2009.2021379

[25] R. M. Pyndiah. Near-optimum decoding of product codes: Block turbo codes. *IEEE Transactions on Communications* **46**(8):1003–1010, 1998. https://doi.org/10.1109/26.705396

[26] I. Tal, A. Vardy. List decoding of polar codes. *IEEE Transactions on Information Theory* **61**(5):2213–2226, 2015. https://doi.org/10.1109/TIT.2015.2410251

[27] H. A. Naman, A. E. Abdelkareem. Self-interference cancellation in underwater acoustic communications systems using orthogonal pilots in IBFD. *Acta Polytechnica* **63**(1):23–35, 2023. https://doi.org/10.14311/AP.2023.63.0023